Magnetoresistive $La_{0.83}Sr_{0.17}MnO_3$ Ceramics by DAAS Technique

S. Yang and C. T. Lin*

Department of Chemistry and Biochemistry, Northern Illinois University, DeKalb, Illinois 60115

K. Rogacki† and B. Dabrowski

Department of Physics, Northern Illinois University, DeKalb, Illinois 60115

P. M. Adams and D. M. Speckman

The Aerospace Corporation, P.O. Box 92957, Los Angeles, California 90009

Received November 25, 1997. Revised Manuscript Received February 10, 1998

Manganese-based perovskites have been successfully synthesized using deposition by aqueous acetate solution (DAAS). This novel technique, which has the potential for depositing large area thin films with high throughput and low cost, involves the preparation of stoichiometric mixtures of metal−acetate precursor solutions, followed by the subsequent firing of these mixtures at relatively low temperature (600 °C) for short periods of time (<100 min), to produce crystalline lanthanum−strontium−manganate (LSMO) materials. For $La_{0.83}Sr_{0.17}MnO_3$ perovskites, varying the firing temperature from 600 to 900 to 1200 °C (while maintaining a constant firing time of 100 min) results in an increase in product crystallite size (from ∼160 to ∼3300 Å), a sharpening and a shift toward higher temperatures of the metallic transition, a decrease in the material resistivity measured at 350 K (by 1 order of magnitude for each temperature studied), and a change in the XRD 2θ peaks consistent with a material phase transition. Lattice parameters, magnetic dependent resistivities, metallic and ferromagnetic transition temperatures, and magnetization values are comparable to those of LSMO materials prepared by much harsher, conventional methods. The advantages of using the DAAS technique for synthesizing manganese-based perovskites, in particular for thin/thick films, will be discussed.

Introduction

The simple perovskite oxides, ABO_3, have many different types of ferroic phases including ferroelectrics, antiferroelectrics, ferroelastics, ferromagnetics, antiferromagnetics, and coupled forms of these. For B-site cations, the Ti/Zr-based oxides are ferroelectric ceramics[1,2] whereas Mn-based oxides are magnetoresistive materials.[3,4] A perovskite system of particular interest is $La_{1-x}A_xMnO_3$ (A = Sr, Ca, Ba) which is insulating at both end points $x = 0$ and $x = 1$, and becomes metallic and ferromagnetic for $0.5 > x > 0.2$.[5] The recent discovery of colossal magnetoresistance[6−8] in $La_{1-x}A_xMnO_3$ has spurred much interest in its mechanism and the potential use of this class of materials in magnetic sensors and read-head applications.

Many chemical methods have been employed for synthesizing manganese-based perovskites. Conventional solid-state syntheses in air[9] utilize stoichiometric precursor mixtures of either oxides or carbonates of the different constituent elements, which are then repeatedly ground and fired at temperatures >1200 °C for a period of days to obtain good perovskite ceramics. For coprecipitation methods,[10] appropriate metal−chloride, −oxide, −carbonate, and/or −nitrate salts are dissolved in water, nitric acid, or hydrochloric acid. The solid precipitates containing the desired stoichiometric quantities of metals (typically metal hydroxides or metal

* To whom correspondence should be addressed.
† On leave from Institute of Low Temperature and Structure Research, Polish Academy of Sciences, Wroclaw, Poland.

(1) Electroceramic Thin Films, Part I: Processing. Auciello, O., Ramesh, R., Guest Eds.; *MRS Bull.* **1996**, *21* (6), 21.
(2) Electroceramic Thin Films, Part II: Device Applications. Auciello, O., Ramesh, R., Guest Eds.; *MRS Bull.* **1996**, *21* (7), 29.
(3) Schiffer, P.; Ramirez, A. P.; Bao, W.; Cheong, S. W. *Phys. Rev. Lett.* **1995**, *75*, 3336.
(4) Mahendiran, R.; Mahesh, R.; Rangavittal, N.; Tewari, S. K.; Raychaudhuri, A. K.; Ramakrishnan, T. V.; Rao, C. N. R. *Phys. Rev.* **1996**, *B53*, 3348.
(5) Wollen, E. O.; Koehler, W. C. *Phys. Rev.* **1955**, *100*, 545.
(6) (a) Rao, C. N. R.; Cheetham, A. K.; Mahesh, R. *Chem. Mater.* **1996**, *8*, 2421. (b) Mahesh, R.; Mahendiran, R.; Raychaudhuri, A. K.; Rao, C. N. R. *J. Solid State Chem.* **1995**, *114*, 297.
(7) (a) Asamitsu, A.; Moritomo, Y.; Arima, T.; Tokura, Y. *Nature* **1995**, *373*, 407. (b) Urishibara, A.; Morimoto, Y.; Arima, T.; Asamitsu, A.; Kido, G.; Tokura, Y. *Phys. Rev.* **1995**, *B51*, 14103.
(8) (a) Jin, S.; McCormack, M.; Tiefel, T. H.; Ramesh, R. *J. Appl. Phys.* **1994**, *76* (10), 6929. (b) von Helmolt, R.; Holzapfel, B.; Schultz, L.; Samwer, K. *Phys. Rev. Lett.* **1993**, *71*, 2331. (c) Chahara, K.; Ohno, T.; Kasai, M.; Kozono, Y. *Appl. Phys. Lett.* **1993**, *63*, 1990.
(9) (a) Jonker, G. H.; van Santen, J. H. *Physica* **1950**, *16*, 337. (b) Jonker, G. H. *Physica* **1956**, *22*, 707.
(10) Valenzuela, R. *Magnetic Ceramics*; Cambridge University Press: Cambridge, 1994; p 48.

S0897-4756(97)00769-2 CCC: $15.00
Published on Web 04/14/1998

nitrates) are produced, and then filtered, washed, and sintered to produce mixed metal−oxide ceramics. However, inhomogeneities in the coprecipitated product, which give an incorrect metal stoichiometry in the final oxide product, can occur using coprecipitation methods. Differential precipitation due to differences in the solubility of the hydroxide or nitrate salts can alter the relative ratios of metals in the precipitate. The incomplete reaction of metal−chloride reactants during the formation of the insoluble nitrates and/or hydroxides can also result in a preferential loss of these metals, since unreacted chloride salts are soluble and will be removed during the washing, filtration, and drying of the precipitate. Conventional sol−gel processing techniques using metal alkoxides as precursors[11] are plagued with problems of imprecise stoichiometries and the necessity to have a strict control over the processing environment. In addition, the precursor solutions are generally unstable and tend to gel quickly.

Recently, we have successfully developed the deposition by aqueous acetate solution (DAAS) technique,[12−16] for making undoped and extrinsic ion-doped lead titanate (PT), lead zirconate titanate (PZT), and lead lanthanum zirconate titanate (PLZT) thin films, powders, and laser "direct write" patterns. This novel process uses aqueous acetate-based metal precursor solutions (i.e., acetates of Pb^{2+}, La^{3+}, Zr^{4+}, and Ti^{4+} dissolved in a solvent mixture of water and acetic acid), which are sonicated, dried to give a cross-linked glassy gel, consolidated at 450 °C, and then fired at 550−650 °C to produce PT, PZT, or PLZT crystalline product. This technique offers many advantages over conventional lead-based ferroelectric perovskite synthesis methods. The metal−acetate precursor solutions are optically clear and stable under ambient laboratory conditions, and intermolecular mixing in the aqueous phase provides a short diffusion path length between reactive constituents. The intermolecular metal−acetate polymerization that occurs during thermal evaporation of solvent facilitates the crystallization of PT, PZT, and PLZT perovskites at relatively low annealing temperatures (550−650 °C), and the precursor solutions can also be formulated to within 1% of the desired stoichiometry. Furthermore, water-soluble acetates or acetylacetonates of various metal dopants are readily available, so that extrinsically ion-doped perovskites can easily be prepared. The mild reaction conditions of this process make it possible for perovskite thin/thick films to be considered for potential integration with state-of-the-art silicon-integrated circuit technology.[15]

In this paper, the success of the DAAS technique in the preparation of ferroelectric ceramics is extended to the synthesis of manganese-based perovskites with a nominal composition of $La_{0.83}Sr_{0.17}MnO_3$. This novel chemical method was used to prepare crystalline lanthanum−strontium−manganate (LSMO) materials under very mild conditions, with firing temperatures as low as 600 °C and firing times as short as 100 min. Structural, transport, and magnetic properties were measured for $La_{0.83}Sr_{0.17}MnO_3$ perovskites that were synthesized by the DAAS technique and fired at different temperatures. For samples prepared at low temperatures, the resistivity and magnetization values are related to the small crystallite size, defect concentration, and structural modifications. Evidence will be given that the DAAS technique produces LSMO materials of equivalent quality to those produced using solid-state methods, yet the DAAS technique is easy, fast, and effective, with mild crystallization conditions suitable for thin/thick film processing.

Experimental Section

Lanthanum acetate hydrate, strontium acetate, and manganese(II) acetate tetrahydrate were purchased from Strem Chemicals, Inc. Exact formula weights of the respective acetate complexes were determined by weighing triplicate samples of each acetate complex into three separate crucibles of known mass, heating the samples slowly to a constant mass (in a period of about 4 h to a final temperature of 900 °C), determining the weights of the respective metal−oxide products, and back-calculating the exact metal content in the original samples. By completing three titers of each precursor, the La:Sr:Mn compositions of the bulk DAAS precursor solutions were formulated with stoichiometry standard deviations of usually less than 1%.

About 0.1 M of 0.83La/0.17Sr/1.0Mn bulk solution was prepared by dissolving stoichiometric amounts of metal acetates of La, Sr, and Mn in a mixture of deionized water and 10−25% acetic acid. The solution was mixed ultrasonically, and the resultant clear mixture was shown to be stable (with no precipitation or gelation) for several months. Powders of $La_{0.83}Sr_{0.17}MnO_3$ were prepared from the bulk solution as follows. The formulated solution was first dried in air at 110 °C where it was observed to undergo gelation after some initial loss of solvent, and this mixture subsequently hardened to a glassy gel. The gel was then pyrolyzed at 600 °C for 6 h to complete decomposition and to drive the organics off the sample. Samples of the resultant powder product were then annealed for 100 min at either 600, 900, and 1200 °C.

Coupled thermogravimetric−differential thermal analysis (TG/DTA) and Fourier transform infrared (FTIR) spectroscopy were undertaken with a Seiko TG/DTA 320 interfaced to a Nicolet Magna-IR 550 FTIR spectrometer on a sample of hardened $La_{0.83}Sr_{0.17}MnO_3$ gel precursor obtained by drying the formulated clear solution at 110 °C. The sample was heated at a rate of 10 °C/min to a final temperature of 1000 °C, which was held for an additional 60 min. FTIR spectra (KBr pellet) were recorded for 0.83La/0.17Sr/1.0Mn precursor gel and powder perovskites using a Bruker Vector 22 FTIR spectrophotometer. Survey scans for determining the effects of temperature on the evolution of crystalline LSMO perovskites were investigated by $\theta-2\theta$ X-ray powder diffraction (XRD) using a Rigaku D/Max-2200 vertical diffractometer. Samples were ground to a fine powder, mixed with silicon grease, and spread on a glass plate. X-ray diffraction patterns were collected in the range 20−60° with 0.04° steps using Cu Kα radiation.

To measure accurate lattice parameters by XRD, National Institute of Standards and Technology (NIST) Standard Reference Material (SRM) #640b silicon powder (2θ/d-spacing standard) was added to the powder samples. The powder mixture was then pressed into a shallow holder (200 μm deep) backed with a zero background plate (ZBP). Samples were analyzed with Cu Kα radiation using a PC computer-controlled

(11) Bahadur, D.; Yewondwossen, M.; Koziol, Z.; Foldeaki, M.; Dunlap, R. A. *J. Phys. Condens. Matter* **1996**, *8*, 5235.
(12) Lin, C. T. Production of PT/PZT/PLZT Thin Films, Powders, and Laser 'Direct Write' Patterns. U.S. patent 5,188,902, February 23, 1993; U.S. patent 5,348,775, September 20, 1994.
(13) Lin, C. T.; Scanlan, B. W.; McNeill, J. D.; Webb, J. S.; Li, L.; Lipeles, R. A.; Adams, P. M.; Leung, M. S. *J. Mater. Res.* **1992**, *7*, 2546.
(14) Lin, C. T.; Li, L.; Webb, J. S.; Lipeles, R. A.; Leung, M. S. *Integr. Ferroelectr.* **1993**, *3*, 333.
(15) Lin, C. T.; Li, L.; Webb, J. S.; Leung, M. S.; Lipeles, R. A. *J. Electrochem. Soc.* **1995**, *142*, 1957.
(16) Li, L.; Lin, C. T.; Leung, M. S.; Adams, P. M.; Lipeles, R. A. *Mater. Res. Soc. Sym. Proc.*, Vol. 361; *Ferroelectric Thin Films IV*, **1995**, pp 209−214.

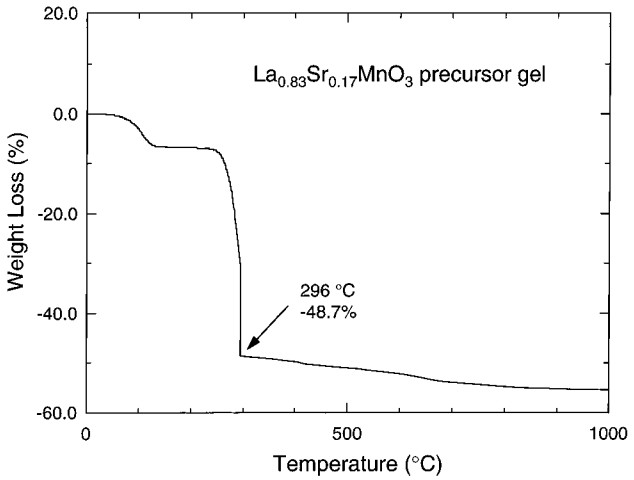

Figure 1. TG/DTA data for $La_{0.83}Sr_{0.17}MnO_3$−acetate gel precursors up to 1000 °C.

Philips Electronics Instruments ADP 3720 vertical powder diffractometer equipped with a θ-compensating slit, diffracted-beam graphite-crystal monochromator, and a scintillation detector. The positions of the Si and LSMO reflections were determined by a profile-fitting technique using a Marquardt nonlinear least-squares algorithm. The positions of the Si reflections were used to construct a correction curve for obtaining accurate 2θ locations for the LSMO reflections. Lattice parameter refinement was performed with a personal computer version of the refinement program of Appleman and Evans.[17] The computer program was forced to accept the Miller indices for the monoclinic $La_{1-x}Sr_xMnO_3$ phase assigned by Hashimoto and co-workers[18] because of potential conflicts with multiply indexed reflections. This was necessary because there otherwise would not have been a sufficient number of independently indexed reflections to perform a refinement.

The electrical resistivity was measured using a standard four-point technique in the temperature range 10−350 K. LSMO samples were cut into bars with approximate dimensions 10 mm × 2 mm × 1 mm. Electrical contacts were established using silver paint. The current densities used in measurements were in the range 1−100 mA/cm^2 depending on the sample's resistivity; smaller current densities were used for more resistive samples. Magnetoresistance (R_H), magnetic susceptibility (χ_{ac}) and magnetization (M) were recorded with a Quantum Design Physical Properties Measurement System equipped with a 7 T superconducting magnet. The R_H and M measurements were performed as a function of temperature, at constant dc bias magnetic field (B) for both zero field cooled (ZFC) and field cooled (FC) samples and as a function of magnetic field at constant temperature. The temperature dependence of χ_{ac} was studied with an ac field of 14 Oe amplitude and 5 kHz frequency.

Results and Discussion

Chemistry of DAAS Process for LSMO Perovskites. The formulated metal acetate solutions containing precursors 0.83La/0.17Sr/1.0Mn are stable at room temperature but were observed to undergo gelation after some initial loss of solvent during drying at 110 °C. Figure 1 displays TG/DTA data for the $La_{0.83}Sr_{0.17}MnO_3$ gelled precursors. Upon heating of the sample, a mass loss initially occurs between 140 and 175 °C, indicating a loss of residual water and acetic acid from the sample as indicated by TG/FTIR analysis. The second and major mass loss, which occurs between 285 and 340 °C, represents the loss of organics and carbon dioxide. There is an additional mass loss above 540 °C that appears to be due to the evolution of CO_2 from the metal oxides.

Surprisingly, a thermally stable compound is formed from metal acetate solutions at temperatures between 175 and 285 °C as shown in Figure 1. It has been proposed[12−16] that the DAAS technique produces polynuclear metal complexes in the aqueous-gel phase, which would allow for strong intermolecular mixing, promote metal−oxygen−metal polymerization during the preannealing phase, and facilitate the crystallization of $La_{0.83}Sr_{0.17}MnO_3$ at relatively low temperatures. It is possible that the thermally stable complex observed at 175 °C in Figure 1 is such a polynuclear metal complex.

Figure 2 shows FTIR spectra of the $La_{0.83}Sr_{0.17}MnO_3$ precursor solution: (a) dried at 110 °C for 4 h, (b) preconsolidated at 280 °C for 2 h, (c) consolidated and annealed at 550 °C for 6 h, and (d) annealed at 900 °C for 100 min. The chemistry for the formation of LSMO perovskite materials by the DAAS technique may be inferred from the FTIR spectral changes observed during each of the DAAS process steps. These results appear to be consistent with a transformation in the coordination chemistry of the acetate ligands of the metal−acetate complexes during drying, consolidation, and annealing. The metal−acetate precursor ligands initially appear to exhibit a mixture of unidentate and bidentate cross-linked structures but convert completely to bidentate structures as the samples are heated, as is indicated by the changes in asymmetric and symmetric stretching modes of the acetate ion. The metal−oxygen bonds of the final product are subsequently organized into a MnO_6 octahedral structure,[19] as evidenced by the appearance of a well-defined spectral band at about 600 cm^{-1}. Nakamoto and co-workers[20] have shown that the frequency separation between asymmetric and symmetric modes of the acetate group is an indication of the nature of the coordination in a related group of acetates. In spectrum 2a, two bands around 1710 and 1280 cm^{-1} can be attributed to the υ_{asym} and υ_{sym} vibrations of the $-COO^-$ group, respectively. The large frequency separation, $\Delta\upsilon$ = 430 cm^{-1}, suggests an unidentate acetate ligand. Two other spectral transitions at 1562 and 1408 cm^{-1}, as shown in spectrum 2a, are also due to the υ_{asym} and υ_{sym} vibrations of the $-COO^-$ group, but $\Delta\upsilon$ = 154 cm^{-1} is consistent with bidentate acetate ligands.[21] The observed bidentate ligand in Figure 2a suggests that the dried and preconsolidated $La_{0.83}Sr_{0.17}MnO_3$ precursor solutions are probably held in a preannealed phase via a strong intermolecular mixing where ordering of a solid network of crystalline structure may be virtually completed. The formation of polynuclear metal complex in the preannealed phase of LSMO precursor solution is further evident in spectrum 2b where the unidentate bands at

(17) Appleman, D. E.; Evans, H. T. Indexing and least-squares refinement of powder diffraction data Geological Survey Computer Contribution, program number W9214.
(18) Hashimoto, T.; Ishizawa, N.; Mitutani, N.; Kato, M. *J. Cryst. Growth* **1987**, *84*, 207.
(19) McDevitt, N. T.; Baun, W. L. *Spectrochim. Acta* **1964**, *20*, 799.
(20) Nakamoto, K.; Fujita, J.; Tanaka, S.; Kobayashi, M. *J. Am. Chem. Soc.* **1957**, *79*, 4904.
(21) von Thiele, K. H.; Panse, M. Z. *Anorg. Allz. Chem.* **1978**, *441*, 23.

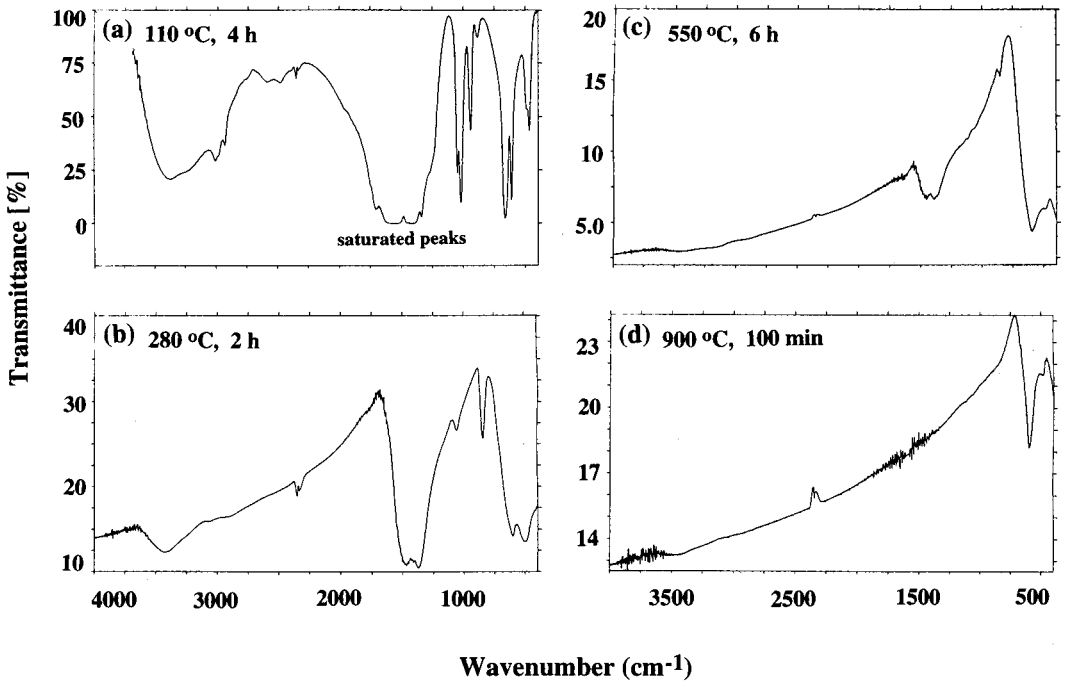

Figure 2. FTIR spectra of $La_{0.83}Sr_{0.17}MnO_3$ precursor solution: (a) dried at 110 °C for 4 h, (b) preconsolidated at 280 °C for 2 h, (c) consolidated and annealed at 550 °C for 6 h, and (d) annealed at 900 °C for 100 min.

1710 and 1280 cm^{-1} disappear completely and the bidentate bands at 1562 and 1408 cm^{-1} dominate.

Figure 2c shows the beginning of developing a spectral band of metal−oxygen vibration at 600 cm^{-1}. The spectral bands, 1548 and 1416 cm^{-1}, belonging to a bridging acetate ligand of polynuclear metal complex become quite weak. These observations indicate that the $La_{0.83}Sr_{0.17}MnO_3$ perovskites begin to crystallize at an annealing temperature as low as 550 °C. When the consolidated LSMO powder is annealed at 900 °C (or a higher temperature at 1200 °C) for 100 min, Figure 2d shows a clean FTIR spectrum with a moderately sharp spectral peak at 600 cm^{-1}. This represents a crystalline powder containing solely the $La_{0.83}Sr_{0.17}MnO_3$ perovskites without a trace of pyrochlore phase impurities.

Effects of Temperature on the Evolution of Crystalline $La_{0.83}Sr_{0.17}MnO_3$ Powder. The transformation of crystalline LSMO perovskite bulk powders should, in principle, depend both on annealing time and temperature. In this study the annealing temperature was varied between 500 and 1200 °C and the annealing times ranged from 10 to 1000 min. Figure 3 illustrates the X-ray diffraction patterns of $La_{0.83}Sr_{0.17}MnO_3$ powders prepared by the DAAS technique as a function of firing temperature. When the annealing schedule was set at 500 °C for 6 h, the resultant $La_{0.83}Sr_{0.17}MnO_3$ powders are purely amorphous as shown by the XRD pattern in spectrum 3a. However, when the LSMO powder was annealed at 550 °C for 6 h the XRD pattern (spectrum 3b) displays distinct crystalline peaks that are similar to, but slightly broader, than those observed for powders annealed at 600 °C for 100 min (spectrum 3c). This indicates that some crystallinity of $La_{0.83}Sr_{0.17}MnO_3$ powder can be achieved at annealing temperatures as low as 550 °C.

To study the effects of temperature, by itself, on the development of crystallinity, the annealing time was kept constant (100 min) while the samples were annealed at 600, 900, and 1200 °C. As the temperature increased from 600 °C (spectrum 3c) to 900 °C (spectrum 3d) the intensities of the XRD peaks increased, the full width at half-maxima (fwhm) of the XRD peaks began to narrow, some peaks began to develop shoulders, and the peaks shifted slightly to lower 2θ. With an annealing temperature of 1200 °C (Figure 3e) the X-ray peaks continued to narrow and many of the reflections became well-resolved doublets (or triplets). Peak shift, combined with doublet formation normally observed for monoclinic structure, could indicate the formation of a new crystalline phase of $La_{0.83}Sr_{0.17}MnO_3$ species at low annealing temperatures. The effects of temperature on the crystal structure transformation can be more clearly seen in expanded views of the selected X-ray reflections in Figure 4. The XRD pattern for the LSMO powder annealed at 1200 °C is in excellent agreement with the pattern of monoclinic $La_{0.8}Sr_{0.2}MnO_3$[18] and with those

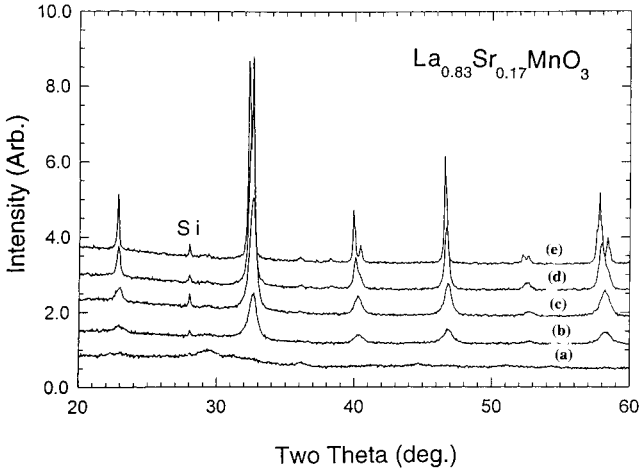

Figure 3. X-ray diffraction patterns of $La_{0.83}Sr_{0.17}MnO_3$ powders fired at (a) 500 °C for 6 h, (b) 550 °C for 6 h, (c) 600 °C for 100 min, (d) 900 °C for 100 min, and (e) 1200 °C for 100 min.

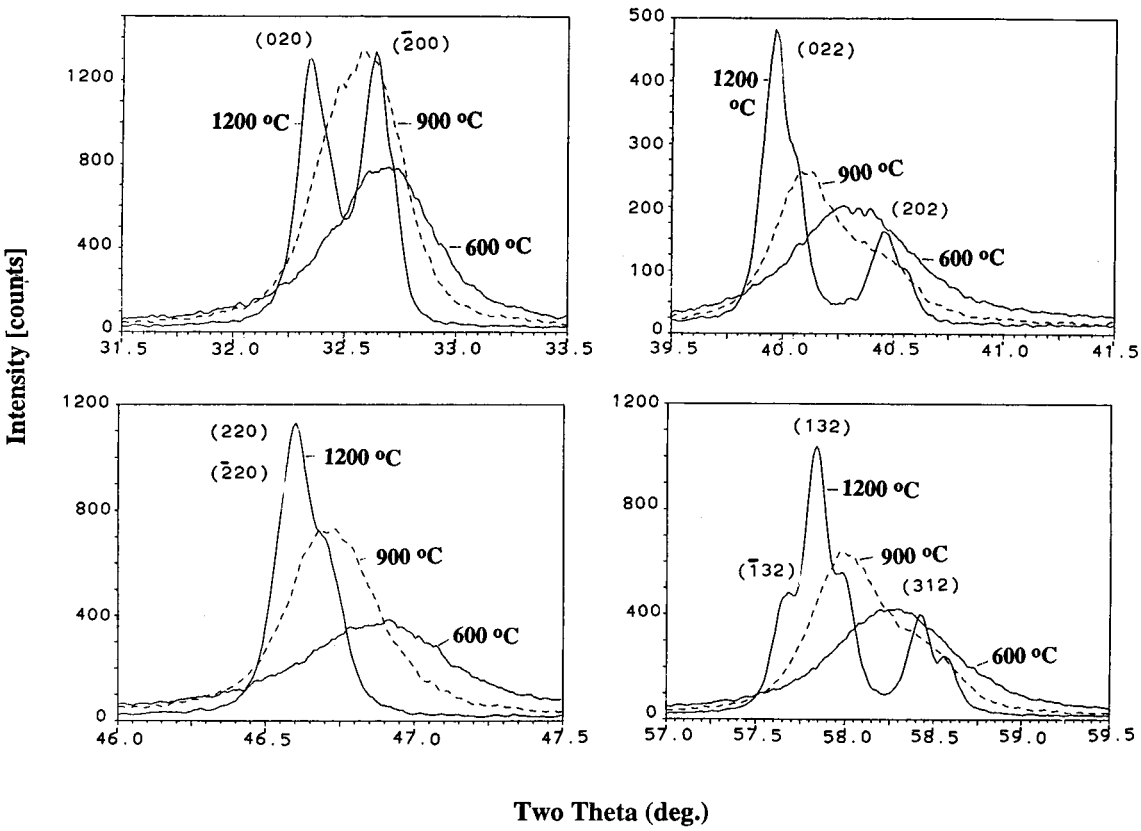

Figure 4. Expanded views of XRD reflections from $La_{0.83}Sr_{0.17}MnO_3$ powders annealed at 600, 900, and 1200 °C for 100 min. Reflections are identified by monoclinic indices.

LSMO materials prepared by much harsher, conventional solid-state methods.[9]

There is considerable confusion in the literature concerning the crystal structure of LSMO with a nominal composition of $La_{0.8}Sr_{0.2}MnO_3$. At least two different rhombohedral unit cells have been suggested based on powder XRD studies,[22,23] in addition to a monoclinic unit cell based on single-crystal studies.[18] In general, the actual powder XRD patterns cited with these various structures appear to be identical. It has also been shown that the crystal structure of $LaMnO_3$ is orthorhombic[18] and that the lattice parameters of $La_{1-x}Sr_xMnO_3$ change with composition, becoming nearly pseudotetragonal for $x > 0.5$.[24] Furthermore, it has been reported that the crystal structure of $La_{1-x}Sr_xMnO_3$ also changes as a function of oxygen stoichiometry.[25] In light of the fact that Hashimoto et al. have performed single-crystal studies, which are more reliable than powder XRD structure determinations, we have indexed our LSMO powders using their monoclinic cell. However, it is noted that the crystals studied by Hashimoto et al. were actually twinned, and therefore a complete structure determination may not have been possible. The lattice parameters refined for the $La_{0.83}Sr_{0.17}MnO_3$ powders annealed at 600, 900, and 1200 °C are listed in Table 1.

It can be seen that at 600 °C the structure of $La_{0.83}Sr_{0.17}MnO_3$ is nearly tetragonal and that with increasing temperature the b_o, c_o, and β lattice parameters increase until they are in close agreement with those reported for single-crystal $La_{0.8}Sr_{0.2}MnO_3$.[18] This change in crystal structure (lattice parameters and fwhm) with annealing temperature is very similar to that reported for $La_{1-x}Sr_xMnO_3$ as x is varied from 0.5 to 0.83,[24] and may represent variations in the composition of the crystalline phase as the firing temperature is raised.

Table 1. Lattice Parameters for the $La_{0.83}Sr_{0.17}MnO_3$ Powders

temp, °C	a_o, Å	b_o, Å	c_o, Å	β, deg
600	5.481 ± 0.001	5.486 ± 0.001	7.730 ± 0.011	90.20 ± 0.06
900	5.481 ± 0.002	5.517 ± 0.001	7.751 ± 0.012	90.36 ± 0.07
1200	5.485 ± 0.001	5.533 ± 0.001	7.794 ± 0.006	90.74 ± 0.03
single crystal[18]	5.4843(1)	5.5349(1)	7.7916(3)	90.746(2)

The fwhm of the XRD reflections shown in Figure 4 is related to both crystallite size and nonuniform strain. If the effects of nonuniform strain can be assumed to be minimal, the Scherrer equation (corrected for instrumental broadening) can be used to calculate the crystallite size. The crystallite sizes for the $La_{0.83}Sr_{0.17}MnO_3$ powders annealed at 600, 900, and 1200 °C (at a fixed firing time of 100 min) were calculated from the (220) reflection since it does not undergo broadening and splitting during the monoclinic transformation. The crystallite sizes calculated for the LSMO powders annealed at 600, 900, and 1200 °C were 160, 415, and 3300 Å, respectively. This clearly indicates that, at a fixed annealing time, the crystallite size increases significantly with annealing temperature. The effect of annealing time on the crystallization of $La_{0.83}Sr_{0.17}MnO_3$ powder was also investigated by fixing the firing tem-

(22) Hammouche, A.; Siebert, E.; Hammou, A. *Mater. Res. Bull.* **1989**, *24*, 367.
(23) Harwood: M. *Proc. Phys. Soc. (London)*, **1955**, *68B*, 586.
(24) Gharbage, B.; Henault, M.; Pagnier, T.; Hammou, A. *Mater. Res. Bull.* **1991**, *26*, 1001.
(25) Takeda, B.; Nakai, S.; Kojima, T.; Kanno, R.; Imanishi, N.; Shen, G. *Mater. Res. Bull.* **1991**, *26*, 153.

perature at 700 °C and varying the annealing time (10, 100, 1000 min). The XRD data indicated that the degree of crystallinity of the $La_{0.83}Sr_{0.17}MnO_3$ powder does not change significantly with respect to the range of annealing time investigated. Thus, the firing temperature is the main controlling factor, and a fully crystalline material can be formed even at firing times as short as 10 min.

Transport Properties of $La_{0.83}Sr_{0.17}MnO_3$ Magnetoresistance Powders. The Mn-based perovskites exhibit a magnetoresistive effect near the ferromagnetic ordering of Mn spins that is accompanied by a large decrease in electrical resistivity when a dc magnetic field is applied.[26] Several studies[8b,9a,26a,27] on Mn-based perovskites, $La_{1-x}A_xMnO_3$ indicated that the Curie temperature T_c becomes the highest when ~30% of the Mn^{3+} is converted to Mn^{4+} by substituting divalent ions, A = Ba, Sr, Ca, and Pb, for La^{3+}. Even for this "hole-doping" range, there are large variations in the observed T_c and the magnitude of the reported magnetoresistance.[7b] These reported discrepancies have been ascribed to chemical disorder,[28] oxygen deficiencies,[29] grain boundary effects,[30] and lattice constant effects.[7b,31]

$La_{1-x}A_xMnO_3$ perovskites were known to undergo gradual structural changes from an orthorhombic phase at $x = 0$ to a monoclinic or rhombohedral phase at $0.1 < x < 0.5$ and finally to a cubic phase at $x > 0.5$.[18,24] The A site doping of Mn-based perovskites by alkaline earth elements is an effective way to control the band filling of the electronically active Mn−O−Mn network.[32] These substitutions have an effect similar to doping with excess oxygen that can modify the crystal structure from orthorhombic to rhombohedral and simultaneously lead to a magnetic transformation from paramagnetic insulator to a ferromagnetic metal. When ~17% of the Mn^{3+} is converted to Mn^{4+}, the T_c is located near 300 K for A = Sr substitution. The colossal magnetoresistive (CMR) effect is usually the largest near T_c. The CMR effect decreases with increasing T_c. Thus, the $x = 0.17$ composition of $La_{1-x}A_xMnO_3$ perovskites was chosen for study because it has the largest CMR near room temperature and has the most practical applications.[7b]

Figure 5 shows the resistivity measurements for $x = 0.17$ (i.e., $La_{0.83}Sr_{0.17}MnO_3$) samples fired at 600, 900, and 1200 °C in air for 100 min, followed by fast cooling to room temperature. Samples display large differences in both the magnitude of the resistivity and its transition temperature dependence on the firing temperature. The resistivity at 350 K decreases by more than 1 order of magnitude for each firing at higher temperatures, i.e., $R = 6.0$, 0.3, and 0.02 Ω cm for firing temperature at 600, 900, and 1200 °C, respectively. The data on temperature dependence of resistivity indicate that transitions to the metallic state on cooling occur at progressively higher temperatures as the firing temperature is increased. While samples fired at 600 and 900 °C show broad transitions to the metallic state at about 150 and 280 K, respectively, the sample fired at 1200 °C displays a sharp transition at 305 K, similar to transitions observed for good quality materials synthesized by solid-state methods.[9]

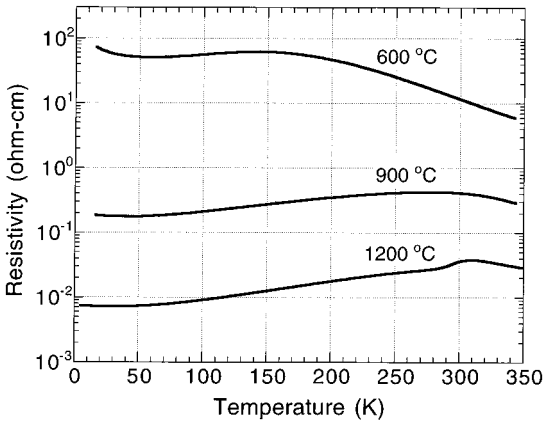

Figure 5. Resistivity as a function of temperature for $La_{0.83}Sr_{0.17}MnO_3$ prepared in air for 100 min at 600, 900, and 1200 °C, followed by fast cooling to room temperature.

The observed transport properties for $La_{0.83}Sr_{0.17}MnO_3$ perovskites, as shown in Figure 5, can be a function of intrinsic (structure and defect concentration) or extrinsic (grain size and grain boundary) properties.[7b,28−31] It appears that the extrinsic cause, the small size of the grains observed for samples synthesized at low temperatures, is the reason for displaying a large magnitude of the resistivity in these samples. As we have shown in the previous section, the crystallite size of $La_{0.83}Sr_{0.17}MnO_3$ perovskites was determined to be about 3300, 415, and 160 Å for powders fired at 1200, 900, and 600 °C, respectively. However, the intrinsic cause should be considered as well. Synthesis of $La_{0.83}Sr_{0.17}MnO_3$ perovskites in air at progressively low temperature increases the amount of vacant sites on both the A (La, Sr) and B (Mn) sites. The presence of these vacant defects on the electronically active Mn−O−Mn network can increase electron scattering and thus, in principle, can also account for the increased magnitude of the resistivity for samples synthesized at low temperatures. However, the concentration of these defect sites is generally small and cannot explain the observed large changes in resistivity as shown in Figure 5. Furthermore, the vacant sites should also increase the amount of Mn^{4+} in $La_{1-x}Sr_xMnO_3$ (i.e., should increase the effective doping level) which is known to decrease the magnitude of the resistivity at low Sr-substitution levels, $x = 0.17$.[7b] Presence of the increased amount of Mn^{4+} was observed in the magnetic measurements (will be discussed in the next section) for samples fired at 900 and 600 °C. It is suggested that the small crystallite size and increased separation of grains is the main reason for large increase of resistivity observed for samples fired at lower temperatures.

Magnetic Properties of $La_{0.83}Sr_{0.17}MnO_3$ Magnetoresistance Powders. Figure 6 displays the mag-

(26) (a) Searle, C. W.; Wang, S. T. *Can. J. Phys.* **1970**, *48*, 2023. (b) Kusters, R. M.; Singleton, J.; Keen, D. A.; McGreevy, R.; Hayes, W. *Physica* **1989**, *B155*, 362.
(27) Jin, S.; Tiefel, T. H.; McCormack, M.; Fastnacht, R. A.; Ramesh, R.; Chen, L. H. *Science* **1994**, *264*, 413.
(28) Rodriguez-Martinez, L. M.; Attfield, J. P. *Phys. Rev. B*, **1996**, *54* (22), 15622.
(29) Ju, H. L.; Gopalakrishnan, J.; Peng, J. L.; Li, Q.; Xiong, G. C.; Venkatesan, T.; Greene, R. L. *Phys. Rev. B* **1995**, *51*, 6143.
(30) Gupta, A.; Gong, G. Q.; Xiao G.; Puncombe, P. R.; Lecoeur, P.; Trouilloud, T.; Wang, Y. Y.; Dravid, V. P.; Sun, J. Z. *Phys. Rev. B* **1996**, *54* (22), 15629.
(31) Hwang, H. Y.; Cheong, S. W.; Radadli, P. G.; Marezio, M.; Batlogg, B. *Phys. Rev. Lett.* **1995**, 75, 914.
(32) Otoshi, S.; Sasaki, H.; Ohnishi, H.; Hase, M.; Ishimaru, K.; Ippommatsu, M.; Higuchi, T.; Miyayama, M.; Yanagida, H. *J. Electrochem. Soc.* **1991**, *138*, 1519.

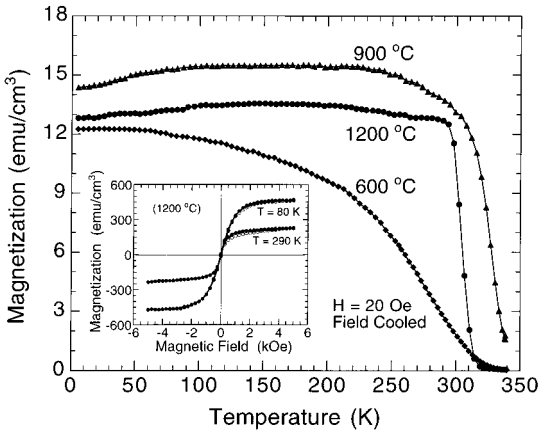

Figure 6. Temperature dependence of the magnetization measured in 20 Oe applied magnetic field (field cooled option) for samples prepared at 600, 900, and 1200 °C. The inset shows the virgin curve (open symbols) and the magnetization loop (closed symbols) measured at 80 and 290 K for sample prepared at 1200 °C.

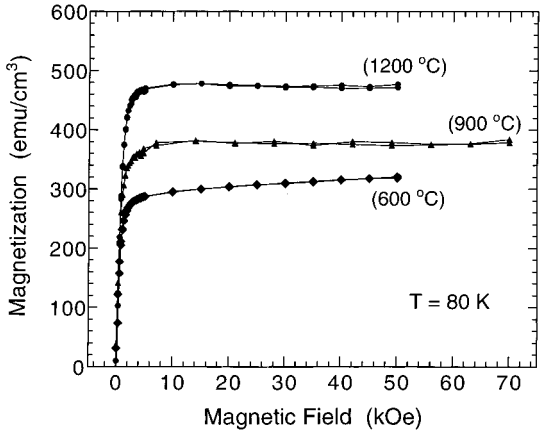

Figure 7. Magnetization measured at 80 K at high magnetic fields for samples prepared at 600, 900, and 1200 °C. The magnetization for sample fired at 600 °C does not saturate even at 5 T magnetic field.

netization as a function of temperature for $La_{0.83}Sr_{0.17}MnO_3$ samples synthesized at 600, 900, and 1200 °C. To precisely define the transition temperature, the magnetization measurements were performed at very small dc bias fields of 20 Oe (field cooled option). The sharp transition from the paramagnetic (PM) to ferromagnetic (FM) state is observed on cooling at the Curie temperature $T_c \approx 305$ K for sample synthesized at 1200 °C, with a small amount of defects. The magnetic transition shown in Figure 6 is matched well with the metal−insulator (M−I) transition detected in Figure 5, indicating the typical CMR effect should be observed for the sample fired at 1200 °C. For samples fired at 600 and 900 °C, the magnetic transitions defined as the temperature of the maximum slope in dM/dT at about 270 and 320 K, respectively (see Figure 6), are broadened and separated from the M−I transitions observed at 150 and 280 K, respectively (see Figure 5). The reason for this separation is not clear at present. It may be caused by the small grain size, defect concentration, or structural modifications.[6a] The magnetization data show that the Curie temperatures are higher than the metal−insulator transition temperatures for samples synthesized at lower temperatures. The increasing of Curie temperatures are caused probably by an increased level of defect dopings owing to the higher density of vacancies formed at 600 and 900 °C. The typical hysteresis loops (magnetization vs magnetic field, $M(H)$) at $T = 80$ and 290 K and the corresponding virgin curves are shown in the inset of Figure 6 for the sample fired at 1200 °C. Both curves are almost identical, indicating that the prepared $La_{0.83}Sr_{0.17}MnO_3$ perovskites display extremely small values of the remnant field.

The saturation magnetization data are shown in Figure 7 for $La_{0.83}Sr_{0.17}MnO_3$ samples synthesized at 600, 900, and 1200 °C. The magnetization for samples prepared at 900 and 1200 °C saturates fully at small magnetic fields of less than 1 T. The average saturation magnetic moments at 5 K are recorded as 2.9 μ_B/Mn and 3.6 μ_B/Mn for samples fired at 900 and 1200 °C, respectively. The increase of the Mn^{3+}/Mn^{4+} ratio toward the expected value 0.83/0.17 (that is, equivalent to the average saturation magnetic moment of 3.83 μ_B/Mn, expected at 0 K) with increasing in sintering

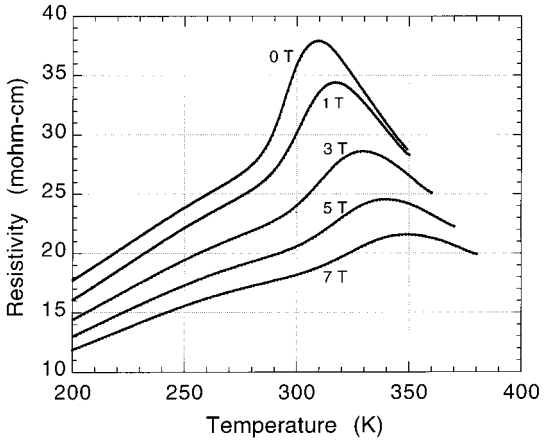

Figure 8. Resistivity as a function of temperature at the magnetic fields $B = 0$, 1, 3, 5, and 7 T (field cooled option) for sample prepared at 1200 °C.

temperature is consistent with the reduction of the vacancy concentration on the A or B sites. The magnetization for the sample prepared at 600 °C does not saturate even at high magnetic fields of 5 T that are commonly observed since any defects can pin spins. The unsaturated magnetization behavior may be due to an imperfect magnetic structure in the $La_{0.83}Sr_{0.17}MnO_3$ sample fired at 600 °C, i.e., inhomogeneous distribution of the Mn^{3+} and Mn^{4+} ions, caused probably by irregular distribution of the vacant sites. The lack of full saturation of magnetization shown in Figure 7 (600 °C) coincides with the broad transition from a PM to a FM state presented in Figure 6 for the $La_{0.83}Sr_{0.17}MnO_3$ sample (fired at 600 °C) at small dc bias field.

The CMR effect was measured for $La_{0.83}Sr_{0.17}MnO_3$ perovskites synthesized by the DAAS method and fired at 1200 °C for 100 min. Figure 8 shows the results for resistivity measurements performed as a function of temperature at several dc magnetic fields. The drop of the resistivity at the M−I transition, observed just below 310 K at 0 T, shifts to higher temperatures when the magnetic field is applied (e.g., to 350 K at 7 T) as a result of the CMR effect. The sharp decrease of the resistivity accompanied by an abrupt increase of magnetization as shown in Figure 6 provides evidence that in this sample the M−I and PM to FM transitions occur simultaneously. The largest CMR effect was observed around

300 K where the relative change in resistivity is $\Delta\rho/\rho_o \sim 20\%$ with application of a 1 T magnetic field. Small magnetoresistance effects are found above the FM transitions in the region of the paramagnetic and insulating states.

Conclusion

Magnetic perovskites of the form $La_{0.83}Sr_{0.17}MnO_3$ have been synthesized using a novel technique, deposition by aqueous acetate solution (DAAS). The crystallite size of these perovskites was determined to be about 3300, 415, and 160 Å for $La_{0.83}Sr_{0.17}MnO_3$ powders fired for 100 min at 1200, 900, and 600 °C, respectively. The small size of the grains observed for samples synthesized at low temperatures is believed to be the cause of the large resistivities in these samples. The nature of a ferromagnetic state for all samples prepared is also evidenced by the observation of typical hysteresis loops. For samples synthesized at 1200 °C, a sharp transition from a PM to a FM state is observed on cooling at the Curie temperature $T_c \approx 305$ K. The largest CMR effect is observed at approximately 300 K where the relative change of resistivity ($\Delta\rho/\rho_o$) is ~20% with application of 1 T magnetic field.

DAAS offers several advantages over conventional synthetic techniques. The aqueous-based chemistry allows for a strong intermolecular mixing of the precursors, the La:Sr:Mn atomic ratio in the precursor solution can be controlled to within 1% of the desired stoichiometry, the metal−acetate solutions of different dopants are easy to formulate and are very stable, and the crystallization conditions are relatively mild (low firing temperature and short annealing time). More importantly, the rheology (i.e., viscosity) of the precursor solutions in DAAS technique is easy to control and modify. All of these factors suggest that the DAAS technique has the potential to deposit thin, thick, and layered-structure films of magnetic perovskites over a variety of large area substrates with high throughput and low cost. Such a capability is of critical importance for a wide range of applications, such as the development of high-density, solid-state magnetic memories. This work is currently under investigation in our laboratory.

Acknowledgment. This work was supported, in part, by the Independent Research and Development program at the Aerospace Corporation, the National Science Foundation, and ONR/ARPA. We thank Mr. Frank Calvagna for technical assistance.

CM970769J